Journal of
Advanced Manufacturing Science and Technology

Investigation on cutting temperature of CFRP in robotic rotary ultrasonic drilling with minimum quantity lubrication

Song DONG, Kan ZHENG*, Wentao ZHANG

School of Mechanical Engineering, Nanjing University of Science and technology, Nanjing 210094, China

Received 10 April 2024; revised 25 April 2024; accepted 8 May 2024; Available online

Abstract

Carbon fiber reinforced polymer (CFRP) is widely used in aircraft manufacturing field because of superior physical and mechanical properties. Millions of connection holes require to be drilled on CFRP material, the cutting damage of holes has crucial effect on the aircraft performance. Robotic rotary ultrasonic drilling (RRUD) as a potential method is proposed to improve the drilling quality. Nevertheless, it is difficult to control the drilling temperature to avoid exceeding the glass transition temperature of the resin matrix in a dry cutting environment during RRUD. The minimum quantity lubrication (MQL) technology can improve cooling conditions and achieve temperature reduction effectively. In this paper, an investigation on cutting temperature during the processing method combining RRUD and MQL (RRUD&MQL) is carried out and a theoretical prediction model is established. Firstly, analysis on RRUD&MQL coupling friction reduction mechanism is conducted with consideration of periodic kinematics characteristic in RRUD and lubrication property of MQL droplets. After that, based on this friction reduction mechanism, thrust force is calculated and cutting temperature model is established. Finally, validation experiments results indicate that analytical cutting temperatures agree well with the experimental value, and the average of relative prediction error is 9.12%.

Keywords: Robotic rotary ultrasonic drilling; Minimum quantity lubrication; Cutting temperature; CFRP; Drilling quality

1. Introduction

Due to its superior strength-to-weight characteristics, high corrosion resistance and low coefficient of thermal expansion, CFRP have been widely used in aircraft manufacturing including the Airbus A380 and the Boeing 787 Dreamliner. [1-6] In the assembly process of CFRP parts, millions of connection holes need to be drilled on body materials. [7-9] Carbon fibers of CFRP may cause poor machinability because of its high hardness and abrasiveness, resin matrix of CFRP is easy to exceed the glass transition temperature and result in serious damage during drilling. [10] So the quality control of holes, especially the control of cutting force and cutting temperature during drilling, is crucially important on the connection reliability and even the flight performance. Currently, robotic drilling is gradually being used by aviation manufacturing enterprises due to its quality consistency, flexibility and phase accuracy. [11-13] Meantime, rotary ultrasonic drilling technology offers numerous benefits, including reduced cutting forces and diminished tool wear. [14-17] Dong and Zheng [18-20] presented a new processing method (RRUD) combining robotic drilling

*Corresponding author. *E-mail address:* zhengkan@njust.edu.cn(Kan ZHENG)
Peer review under responsibility of Editorial Committee of JAMST
DOI: 10.51393/j.jamst.2025001

and RUD. From previous investigation, both chatter suppression and drilling force reduction is achieved by adopting ultrasonic vibration during robotic drilling.

However, owing to the openness of the robotic drilling device, cutting fluid cooling cannot be used during the RRUD process, causing drilling temperature hard to control. MQL technology provides conditions for processing areas cooling in open environment, and have been widely investigated. Abhishek and Soumya [21] presented that MQL exerts a significant impact on offering efficient lubrication during micro-drilling processes. They proposed an analytical model to determine flow rate of MQL. Pradeep and Samuel [22] designed cost-effective MQL systems for utilizing waste cooking oil in their applications. And with this MQL system, they observed a consistent drilling process. Zhu et al. [23] demonstrated that employing MQL while drilling aluminum alloy AA2024 could reduce the temperature differential between the drill center and the outer corner in contrast to dry and air cooling methods.

Thus, a new processing method combining RRUD and MQL is proposed in this paper, trying to further expand the advantages of both technologies. However, until now, there has been a lack of research on the coupling friction reduction mechanism and cutting temperature model during RRUD&MQL. This paper firstly conducts an investigation on the cutting temperature of CFRP in robotic rotary ultrasonic drilling with minimum quantity lubrication. The paper is structured into four main sections. After this introduction section, Section 2 shows the methodology for developing the analytical model for the cutting temperature. Section 3 presents validation experiments of RRUD&MQL aimed at corroborating the accuracy of the theoretical model. Finally, Section 4 concludes the study.

2. Analysis of cutting temperature

2.1. RRUD&MQL coupling friction reduction mechanism

The kinematic characteristics of RRUD is significantly different from robotic conventional drilling (RCD). The dynamic mode of RRUD is illustrated as Fig.1(a). The movement of the RRUD tool tip comprises a blend of rotation, feeding, and ultrasonic vibration, as illustrated in Fig.1(b). Therefore, the trajectory of the tool tip's motion can be depicted as

$$\begin{cases} S_x(t) = R\cos(\omega t) \\ S_y(t) = R\sin(\omega t) \\ S_z(t) = v_f t + A\sin(2\pi F t) \end{cases} \quad (1)$$

where R is the radius of drill bit (mm), ω is the angular velocity (rad/s)，v_f is the feed rate (mm/s), A is the ultrasonic vibration amplitude (μm), F is the ultrasonic vibration frequency (Hz), and t is the time (s).

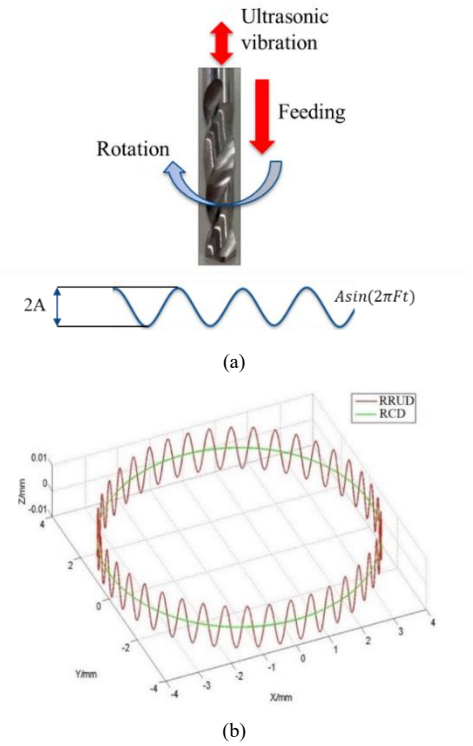

Fig. 1. Kinematic features of RRUD process.

From Fig.1, it can be seen that separated cutting process could achieve in RRUD due to the periodic kinematics characteristic of cutter tooth. Defining the vacant time and cutting time in an ultrasonic vibration period (T) are t_v and t_c respectively. The proportion of cutting time (H) can be described as

$$H = \frac{t_c}{T} = t_c \cdot F \quad (2)$$

Through Eq.(2), when $0 < H < 1$, separated cutting state between drill bit and CFRP drilling surface is obtained. Meantime, the smaller the value of H, the better the separation effect. Based on Li's analysis [24], the critical separation condition of ultrasonic drilling can be presented as Eq.(3), where i is cutting edge number of drill bit. Generally, the number of twist drill teeth is 2.

$$\frac{\pi v_f}{30\omega \cdot i} < 2A \quad (3)$$

This separation phenomenon between drill bit cutting edge and workpiece during RRUD is significant to the lubrication effect of MQL. As seen in Fig.2, in the initial cutting stage, cutting edge squeezes the carbon fiber and always maintain contact with the workpiece material. So the MQL droplets cannot enter the cutting area, friction reduction effect is not achieved. As the cutting edge continues to move along the cutting direction, fiber shearing is occurred as shown in Fig.2(b). Subsequently entering the tool-workpiece stage (Fig.2(c)), with assistance of ultrasonic vibration, the fiber cutting angle is optimized and the chips can be discharged smoothly. [25]

At this point, MQL droplets penetrate into the cutting area and a small portion evaporates when exposed to heat. The remaining part is retained, and these droplets will have a good lubrication and friction reduction function in RRUD process. Meantime, under the action of ultrasonic cavitation, MQL droplets become more uniform and smaller. The friction reduction effect will be further improved (Fig.2(d)).

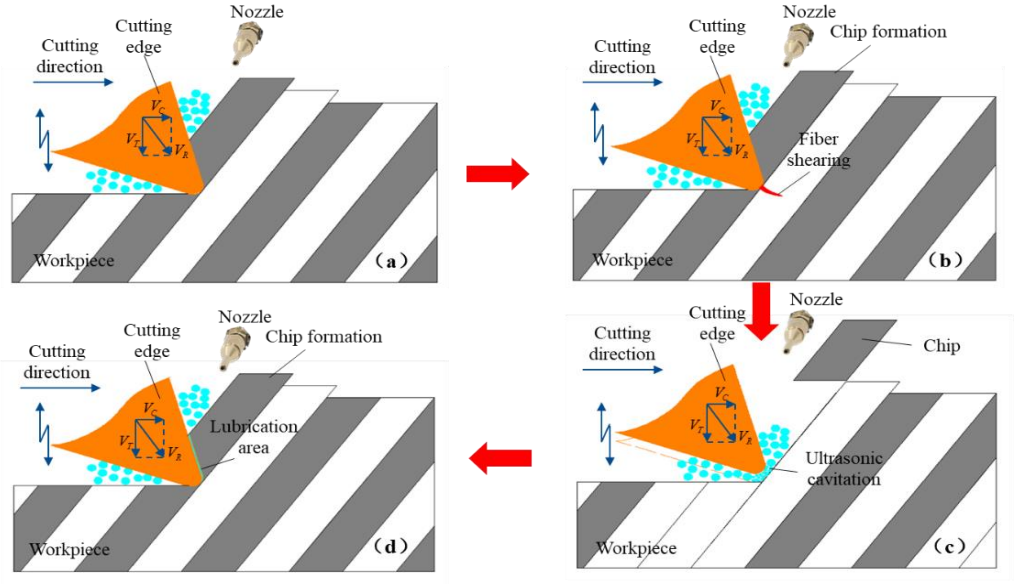

Fig. 2. RRUD&MQL coupling friction reduction effect.

According to the study of Ji [26], MQL friction coefficient (μ_s) using boundary lubrication theory in conventional machining is presented as Eq.(4), where t_b is the effective lubricant film thickness, c_1 is the friction coefficient in the case of dry cutting. c_2 and c_3 are the reference coefficient affected by the shear strengths at the lubricant film contact area and the yield pressure of workpiece material contact area. a_s is the approach of two surfaces.

$$\mu_s = \frac{c_1 a_s^3 + c_2 c_3 \left[\left(a_s + t_b \right)^3 - a_s^3 \right]}{a_s^3 + c_2 \left[\left(a_s + t_b \right)^3 - a_s^3 \right]} \tag{4}$$

Obviously, with the help of ultrasonic vibration, MQL droplets are easier to enter the processing area, thereby improving the lubrication effect of MQL. It will inevitably further reduce the friction coefficient. Considering the proportion of separation time, the friction coefficient for RRUD&MQL coupling process (μ_{RM}) can be calculated as

$$\mu_{RM} = \left(1 - \frac{\pi v_f}{60 A \omega i} \right) \cdot \frac{c_1 a_s^3 + c_2 c_3 \left[\left(a_s + t_b \right)^3 - a_s^3 \right]}{a_s^3 + c_2 \left[\left(a_s + t_b \right)^3 - a_s^3 \right]} \tag{5}$$

2.2. Modeling on cutting temperature

Cutting temperature generation is mainly caused by the axial force work in drilling process. It is essential to construct a thrust force model before temperature modeling. Therefore, the temperature model is created in two stages: "RRUD&MQL parameters to drilling force" and "drilling force to cutting temperature"

2.2.1. RRUD&MQL parameters to thrust force

2.2.1.1. Force generated by the main cutting edge

To account for the distinctive roles of the cutting edge and chisel edge, it is necessary to analyze the forces acting on them individually. Following the Oxley orthogonal cutting model [27], the cutting region along the cutting edge can be classified into two distinct regions: the chip formation region and the scratching region, as illustrated in Fig.3.

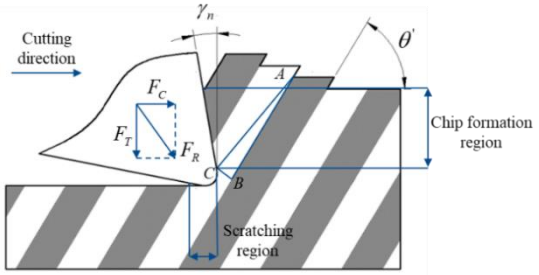

Fig. 3 Action regions caused by cutting edge.

I. Chip formation region

Fig.3 provides an illustration of the decomposition of the total cutting force into two components: F_C, which acts parallel to the cutting speed, and F_T, which acts perpendicular to the cutting speed. Previous research findings indicate that the thrust force in the chip formation region can be described as

$$F_{\mathrm{th}}^{1}=2\int_{a}^{b}\tau_{2}\cdot a_{\mathrm{c}}\cdot\frac{\sin\theta^{'}-\tan(\theta^{'}+\beta-\gamma_{\mathrm{n}})\cdot\cos\theta^{'}}{\frac{\tau_{2}}{\tau_{1}}\tan(\theta^{'}+\beta-\gamma_{\mathrm{n}})\cdot\cos\theta^{'}-\sin\theta^{'}}\cdot\sqrt{1-\frac{w^{2}}{r^{2}}}\mathrm{d}r \tag{6}$$

$$\begin{cases} a=\dfrac{w}{\sin\psi} \\ m=R \end{cases} \tag{7}$$

where τ_1 and τ_2 are respectively the shear strength vertical to the fiber orientation and parallel to the fiber orientation. a_c is the axial uncut chip thickness. $\theta^{'}$ is the equivalent fiber orientation. β is the friction angle and γ_n is the normal rake angle of drill bit. w is the half chisel thickness. r is the distance to the tool center. ψ is the chisel angle.

II. Scratching region

Meanwhile, referring to Fig.3, it becomes apparent that the friction force results from the extrusion between flank face and CFRP workpiece. Following Hertz contact theory [28] , this element of contact force can be computed as

$$\mathrm{d}P_{h}=\frac{\pi r_{\mathrm{e}}E_{3}}{8(1-\nu^{2})}\mathrm{d}l \tag{8}$$

where r_e represents the fillet radius of the cutting edge, E_3 denotes the elastic modulus in the thickness direction, and v represents the Poisson's ratio of CFRP. As established in section 2.1, the friction coefficient for the RRUD&MQL coupling process is obtained from Eq.(5). Consequently, the expression for the friction force in the scratching region can be given as

$$\mathrm{d}F_{\mathrm{f}}=\mu_{\mathrm{RM}}\mathrm{d}P_{\mathrm{h}} \tag{9}$$

The friction force can be decomposed into vertical and horizontal components, with the vertical component calculated as

$$\mathrm{d}F_{th}^{2}=\left(\cos\theta-\mu_{\mathrm{RM}}\sin\theta\right)\frac{\pi r_{\mathrm{e}}E_{3}}{8(1-\nu^{2})}\mathrm{d}l \tag{10}$$

Based on previous research findings, the length element (dl) of the cutting edge can be calculated using the Eq. 11, where p stands for half of the rake angle.

$$\mathrm{d}l=\frac{\mathrm{d}r}{\sin p}\sqrt{1-\frac{w^{2}}{r^{2}}} \tag{11}$$

Therefore, thrust force in scratching region region can be expressed as

$$F_{\mathrm{th}}^{2}=2\int_{m}^{b}\left(\cos\theta-\mu_{\mathrm{RM}}\sin\theta\right)\frac{\pi r_{\mathrm{e}}E_{3}}{8(1-\nu^{2})\sin p}\cdot\sqrt{1-\frac{w^{2}}{r^{2}}}\mathrm{d}r \tag{12}$$

2.2.1.2. Force generated by the chisel edge

When drilling CFRP, the chisel edge initially applies pressure to the composite material, followed by the cutting edge making contact and initiating the cutting process. As the drill bit undergoes axial feed and circumferential rotation, the squeezing depth of the chisel edge into the CFRP increases, resulting in the squeezing of the composite material towards the side of the chisel edge.

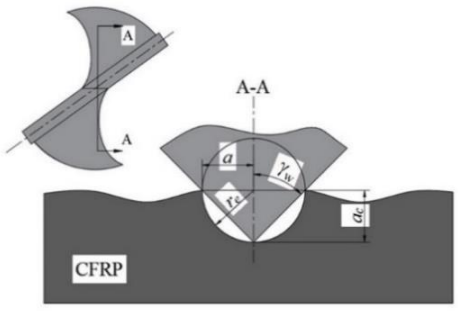

Fig. 4. Force analysis on chisel edge.

Fig. 4 illustrates a cross-section between chisel edge and workpiece during drilling process. In order to streamline the model, the area where the chisel edge penetrates the CFRP material is considered as a rigid wedge. Additionally, pressing portion is simplified into a cylindrical shape (r_e). Based on theory of Hertz contact [28] , the force by chisel edge can be expressed as Eq.(13). The value of r_e can be determined using Eq.(14). The width of pressing part, denoted as a, can be expressed as stated in Eq.(15). Furthermore, the chisel diameter, represented as $d^{'}$, is defined as $d^{'}=2w/\sin\psi$. v signifies Poisson's ratio, E_3 is elastic modulus through thickness direction of CFRP.

$$F_{\mathrm{chi}}=\frac{\pi a^{2}E_{3}}{4(1-\nu^{2})r_{\mathrm{e}}}d^{'} \tag{13}$$

$$r_{\mathrm{e}}=\frac{a_{\mathrm{c}}}{2\cos^{2}\gamma_{\mathrm{w}}} \tag{14}$$

$$a=a_{\mathrm{c}}\tan\gamma_{\mathrm{w}} \tag{15}$$

By substituting Eq.(14) and (15) into Eq.(13), we can express the thrust force on the chisel edge during CFRP drilling as

$$F_{\mathrm{chi}}=\frac{\pi a_{\mathrm{c}}E_{3}\sin^{2}\gamma_{\mathrm{w}}}{2(1-\nu^{2})}d^{'} \tag{16}$$

Hence, the thrust force can be determined by integrating the forces acting on both the cutting edge and the chisel edge, as represented in Eq.(17).

$$\begin{aligned} F_{\mathrm{th}}&=F_{\mathrm{th}}^{1}+F_{\mathrm{th}}^{2}+F_{\mathrm{chi}} \\ &=2\int_{m}^{b}\tau_{2}\cdot a_{\mathrm{c}}\cdot\frac{\sin\theta^{'}-\tan(\theta^{'}+\beta-\gamma_{\mathrm{n}})\cdot\cos\theta^{'}}{\frac{\tau_{2}}{\tau_{1}}\tan(\theta^{'}+\beta-\gamma_{\mathrm{n}})\cdot\cos\theta^{'}-\sin\theta^{'}}\cdot\sqrt{1-\frac{w^{2}}{r^{2}}}\mathrm{d}r \\ &\quad+2\int_{m}^{b}\left(\cos\theta-\mu_{\mathrm{RM}}\sin\theta\right)\frac{\pi r_{\mathrm{e}}E_{3}}{8(1-\nu^{2})\sin p}\cdot\sqrt{1-\frac{w^{2}}{r^{2}}}\mathrm{d}r \\ &\quad+\frac{\pi a_{\mathrm{c}}E_{3}\sin^{2}\gamma_{\mathrm{w}}}{2(1-\nu^{2})}d^{'} \end{aligned} \tag{17}$$

2.2.2. Thrust force to cutting temperature

During the RRUD process, thrust force doing work is the fundamental reason for the generation of cutting temperature. From Fig.2(a), the rotary linear velocity is perpendicular to the thrust force direction, so the linear velocity has no effect on the work done by the

thrust force. And linear velocity generated by ultrasonic vibration and feed rate play a dominant role in work done by the thrust force. Based on RRUD tool kinematic analysis (Eq.(1)), the axial velocity expression of the tool can be obtained as

$$v_t = \dot{S}_z(t) = v_f + 2\pi FA\cos(2\pi Ft) \tag{18}$$

So the the power output of thrust force according to Newton's second law can be expressed as

$$P_t = F_{th} \cdot v_t = F_{th} \cdot \left[v_f + 2\pi FA\cos(2\pi Ft)\right] \tag{19}$$

After that, the heat flux density can be achieved as

$$h = \frac{p_t \chi}{T_e A_h} = \frac{F_{th} v_t \chi}{T_e A_h} \tag{20}$$

where χ is the proportional coefficient of heat transfer to the workpiece, T_e is the Thermal equivalent, T_e =4.1840 J/cal, A_h is the contact area between the drill bit and the cutting area. According to the analysis of the geometric characteristics of the tool, the area of the heat source area is

$$A_h = \frac{d\sin\psi - 2w(\cos\psi - \sin p)}{\sin\psi \sin p} \tag{21}$$

Lastly, highest temperature in the cutting area can be calculated by using a temperature field algorithm with continuous infinite heat sources as

$$T_h = \frac{h}{\kappa_1} \cdot \sqrt{\frac{4\kappa_1 t_r}{c_s \rho_c \pi}} \tag{22}$$

where κ_1 is the thermal conductivity, t_r is the time of temperature rise, c_s is the specific heat capacity and ρ_c is the material density.

3 Experimental verification

3.1. Experiments platform setup

Temperature measurement experiments during RRUD process are carried out using the system illustrated as Fig.5. Drilling experiments are carried out on an industrial robot (KUKA KR500 2830MT). The rotary ultrasonic drilling system is mainly consisted of ultrasonic generator and ultrasonic tool holder. According to the designed structure of this system, the frequency is 25.2 kHz, the stable amplitude is 6.0 μm when the tool overhang length is 35 mm. In this investigation, an infrared thermal imager (FLIR A615) is used for drilling temperature measurement, whose image frequency is 50 Hz, measurement range is -20-2000 °C and measurement accuracy is ±2 °C. Drill bit applied in the experiments is a 4.5 mm cemented carbide twist drill, and the specific parameters are as table 1. CFRP workpiece is selected as CCF300 with 600 mm×400 mm×4 mm for drilling, the mechanical-physical properties is listed in Table 2.

Meantime, the MQL equipment composition and principle is shown as Fig.6. The lubricating liquid in the storage tank is transported to the mixing chamber through an oil pump. In the atomization chamber, lubricating liquid is atomized by a high-pressure and high-speed air jet from the compressor. Then, it enters the nozzle to inject gas-liquid flow into the processing area, achieving cooling and lubrication effects. In the drilling process, the distance between nozzle and workpiece is set as 25 mm, pressure given by air compressor is 0.8 MPa, lubricating liquid flow is 1.5 ml/min.

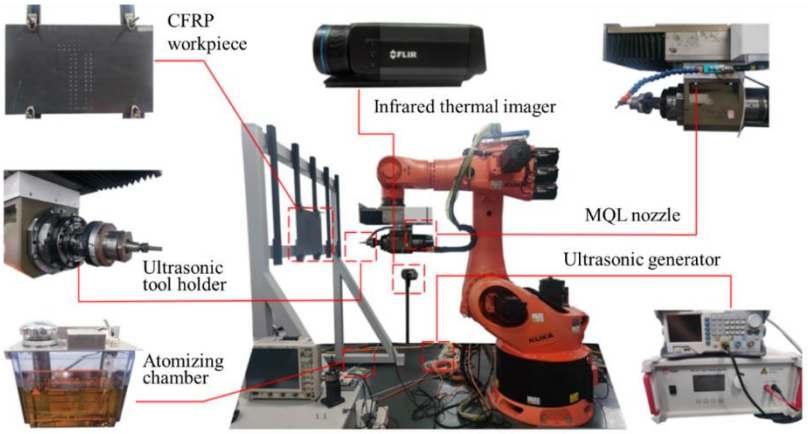

Fig. 5. Experimental platform of RRUD with MQL.

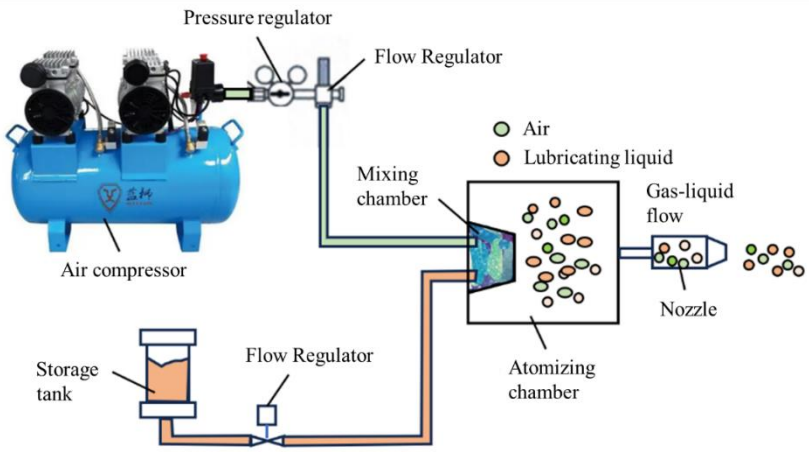

Fig. 6. MQL equipment composition and principle.

Table 1 Parameters of the tool.

Parameter	Value	Parameter	Value
$2R$	4.5 mm	$2w$	0.81 mm
p	59°	γ_w	30°
ψ	54°	γ_f	15°
β	30°		

Table 2 Mechanical-physical properties of CFRP.

Parameter	Value	Parameter	Value
E_3	3.32×10^3 MPa	ρ_c	1.76 g/cm^3
τ_1	90 MPa	Tensile strength	3950 MPa
τ_2	44.2 MPa	Elongation	1.7%
v	0.3		

3.2. Experiments design

In order to compare the drilling temperatures during three processing methods (RCD, RRUD, RRUD& MQL), single factor experiments are conducted. Based on drilling experience and spindle capacity, factors and their respective levels are established as outlined in Table 3. After drilling, hole wall surfaces are observed by SEM. To minimize measurement errors caused by accidental factors, each experiment is repeated 3 times and the mean is taken as the measurement value.

Table 3 Experimental factors and levels.

Factors	Unit	Level				
		A	B	C	D	E
Spindle speed	r/min	1000	2000	3000	4000	5000
Feed rate	mm/min	40	60	80	100	120
Amplitude	μm	0	6	-	-	-

3.3. Experimental results and model verification

The results of cutting temperature by infrared thermal imager illustrated as Fig.7. As CFRP matrix resin is temperature sensitive. When the temperature exceeds its glass transition temperature (T_g is ranged from 150-180 ℃), the resin will undergo softening, burning, or degradation, leading to a decrease in the bonding strength between the matrix and reinforcement, and a sudden decrease in the mechanical properties of the material. Thus, taking the maximum temperature in the drilling area as the measured value in this paper.

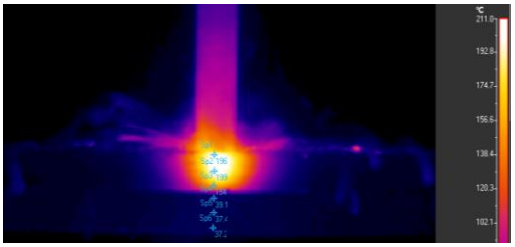

Fig. 7. Results of cutting temperature by infrared thermal imager.

Fig.8 indicates the comparison of cutting temperature using three processing methods (RCD, RRUD, RRUD&MQL). While ultrasonic amplitude is equal to zero, RRUD is changed to RCD. From Fig. 8, cutting temperature of RRUD is close to those of RCD. The role of ultrasonic vibration in the cutting temperature of CFRP is not obvious in robotic drilling. This reason is that although ultrasonic vibration improves heat dissipation conditions, but heat generation also increases by the high-frequency friction on the tool flank face, so ultrasonic vibration doesn't has significant effect on reducing cutting temperature.

On the other hand, it can be found that cutting temperatures obviously decrease during RRUD& MQL. RRUD&MQL coupling friction reduction has crucial effect on the control of thermal damage as shown in Fig.9 (Ω=3000 r/min). From the surface morphology of hole wall observed by SEM, the hole wall of CFRP is seriously damaged in RCD, defects such as resin burn, matrix deboning and fiber pull-out

are occurred. In RRUD, the number of hole wall damage is improved, but there are still serious defects such as resin burn and fiber pull-out. In process of RRUD&MQL, hole wall surface becomes smooth, only a small amount of slightly tool scratches exists. This trend is consistent with the analysis in section 2.1.

The relationship between spindle speed and cutting temperature is illustrated in Fig.8(a). Cutting temperature rises with the increasing of spindle speed. This is because the number of tool rotations per unit time increases at higher spindle speed and therefore heat generated by flank face friction rises drastically. It deteriorates the cutting temperature. The relationship between feed rate and drilling temperature is expressed as Fig.8(b). It can be found that, when the feed rate increases, the temperature rises accordingly. This phenomenon primarily arises due to the increase in the thickness of uncut chip, thrust force increases quickly resulting in the rise of drilling temperature.

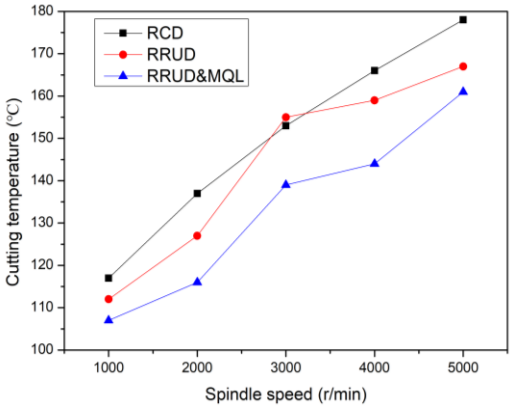

(a) Effect of spindle speed on the cutting temperature

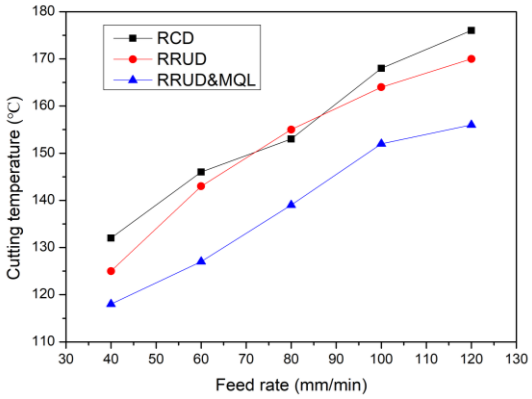

(b) Effect of feed rate on the cutting temperature

Fig. 8. Comparison of cutting temperature under three processing methods.

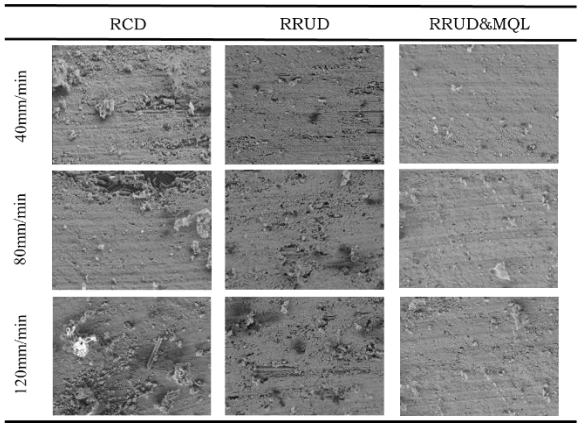

Fig. 9. Comparison of thermal damage under three processing methods.

By incorporating the processing parameters and material properties of CFRP into the theoretical model (Eq.(22)), the predicted values of cutting temperature can be obtained. Table 4 lists the values of theoretical results and experimental results. The temperature comparison between the predictive and experimental values is illustrated as Fig.10. The trend of theoretical values is consistent with the trend achieved from experiments. Meantime, relative error of theoretical model is shown as Fig.11. The range of relative error is 5.62%-12.69%. All experimental groups were within an acceptable range (15%), with an average of 9.12%.

Table 4 Experimental results and theoretical results of temperature (unit: ℃).

No.	Experimental results			Theoretical results
	RCD	RRUD	RRUD& MQL	RRUD& MQL
1	117.29	112.91	107.32	99.98
2	137.07	127.25	116.69	127.62
3	153.95	155.76	139.54	121.84
4	166.14	159.28	144.15	156.28
5	178.36	167.64	161.85	173.84
6	132.48	125.33	107.92	113.98
7	146.77	143.02	116.25	106.15
8	153.69	155.46	139.24	122.07
9	168.24	164.95	144.39	156.27
10	176.18	170.35	161.08	179.85

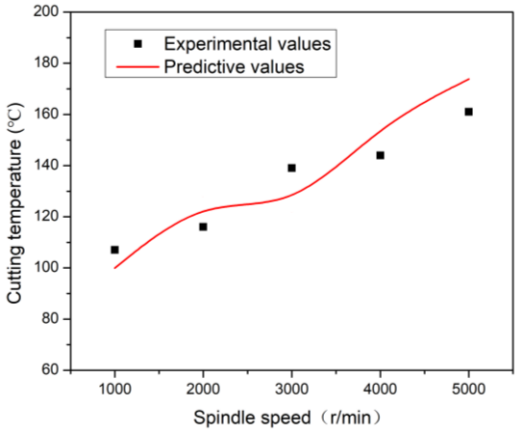

(a)

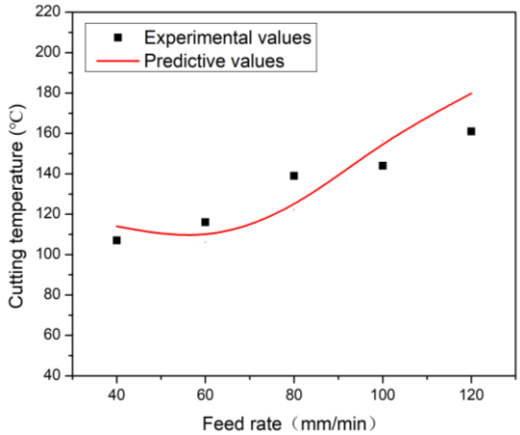

(b)

Fig. 10. Comparison of cutting temperature between theoretical values and experimental values.

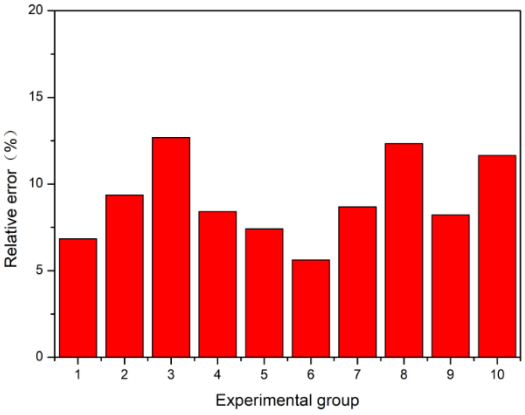

Fig. 11. Relative error of theoretical model.

4. Conclusion

In this paper, an investigation on drilling temperature during RRUD&MQL process is conducted and a theoretical model is proposed in RRUD&MQL of CFRP. Through verification experiments, the calculated temperature agrees well with the experimental value. The following conclusions can be obtained from this study:

(1) Cutting temperatures obviously decrease during RRUD&MQL. RRUD&MQL coupling friction reduction has crucial effect on the control of thermal damage.

(2) The model proposed in this paper provides a mathematical approach for forecasting the cutting temperature in the RRUD&MQL process of CFRP. RRUD parameters, MQL parameters, drill bit parameters and mechanical properties of CFRP are all considered.

(3) The results of validation experiments indicate that calculated temperatures are agreed with experimental values, and the average of relative prediction error is only 9.12%.

Acknowledgements

This work was supported by the National Natural Science Foundation of China (No. 52305472), the Project on the Technological Leading Talent Teams Led by Frontiers Science Center for Complex Equipment System Dynamics (No. FSCCESD220401) and the Jiangsu Funding Program for Excellent Postdoctoral Talent (No. 2022ZB264).

References

1. Cao SY, Li HN, Huang WJ, et al. A delamination prediction model in ultrasonic vibration assisted drilling of CFRP composites. *J Mater Process Tech* 2022;302(1):117480.
2. Cao SY, Li HN, Tan GF, et al. Bi-directional drilling of CFRPs: From principle to delamination suppression. *Compos Part B-Eng* 2023;248(1): 110385.
3. Zhu WY, Fu HG, Li F, et al. Optimization of CFRP drilling process: a review. *Int J Adv Manuf Technol* 2022;123(5-6):1403-32.
4. Feito N, López-Puente J, Santiuste C, et al. Numerical prediction of delamination in CFRP drilling. *Compos Struct* 2014;108(1):677-83.
5. Li SJ, Li QQ, Dai LY, et al. Formation mechanism of outlet damage in interlaminar drilling of CFRP. *Int J Adv Manuf Technol* 2023;129(11-12):5117-33.
6. Sun ZF, Geng DX, Meng FX, et al. High performance drilling of T800 CFRP composites by combining ultrasonic vibration and optimized drill structure. *Ultrasonics* 2023;134(1):107097.
7. Fu PQ, Wang Y, Miao YH, et al. Theoretical analysis and experimental research on the pressing force of robot drilling CFRP sheet. *Int J Adv Manuf Technol* 2022;122(1):1-16.
8. Zhang C, Wang XX, Silberschmidt VV. Longitudinal-torsional complex-mode ultrasonic actuator for vibration-assisted drilling of CFRP. *Mach Sci Technol* 2022;26(5):894-921.

9. Zhao M, Wang FJ, Fu R, et al. Drilling study on CFRP/Al stack with different CFRP thickness using chip-breaking step drill bit. *J Manuf Process* 2023;90(1):300-9.
10. Fernández-Pérez J, Díaz-Álvarez J, Miguélez MH, et al. Combined analysis of wear mechanisms and delamination in CFRP drilling. *Compos Struct* 2021;255(1):112774.
11. Abdulla A, Mohamad H, Dewald S, et al. Neuromorphic vision based control for the precise positioning of robotic drilling systems. *Robot Cim-Int Manuf* 2023;79(1):102419.
12. Bu Y, Liao WH, Tian W, et al. Stiffness analysis and optimization in robotic drilling application. *Precis Eng* 2017;49(1):388-400.
13. Gao YH, Wu D, Nan CG, et al. Normal direction measurement in robotic drilling and precision calculation. *Int J Adv Manuf Tech* 2015;76(5-8):1311-8.
14. Li YX, Jiao F, Zhang ZQ, et al. Mechanical drilling force model for longitudinal ultrasonic vibration-assisted drilling of unidirectional CFRP. *J Mater Process Tech* 2023;319(1):118091.
15. Lotfi M, Amini S. Experimental and numerical study of ultrasonically-assisted drilling. *Ultrasonics* 2017;75(1):185-93.
16. Wang JJ, Zhang JF, Feng PF, et al. Experimental and theoretical investigation on critical cutting force in rotary ultrasonic drilling of brittle materials and composites. *Int J Mech Sci* 2018;135(1):555-64.
17. Chang SSF, Bone GM. Burr size reduction in drilling by ultrasonic assistance. *Robot Cim-Int Manuf* 2005;21(4-5):442-50.
18. Dong S, Zheng K, Liao WH. Stability of lateral vibration in robotic rotary ultrasonic drilling. *Int J Mech Sci* 2018;145(1):346-52.
19. Dong S, Liao WH, Zheng K, et al. Investigation on exit burr in robotic rotary ultrasonic drilling of CFRP/aluminum stacks. *Int J Mech Sci* 2019; 151(1):868-76.
20. Dong S, Liao WH, Zheng K. Investigation on thrust force in rotary ultrasonic drilling of CFRP/ aluminum stacks. *P I Mech Eng C-J Mec* 2020; 234(2):394-404.
21. Abhishek S, Soumya G. Evaluation of adequacy of lubricants in MQL micro-drilling by a developed analytical model and experiments. *J Manuf Process* 2023;101(1):1592-604.
22. Pradeep KG, Samuel RD. Machinability and tribological analysis of used cooking oil for MQL applications in drilling AISI 304 using a low-cost pneumatic operated MQL system. *J Manuf Process* 2023;104(1):348-71.
23. Zhu ZJ, He BW, Chen JX. Evaluation of tool temperature distribution in MQL drilling of aluminum 2024-T351. *J Manuf Process* 2020;56(1):757-65.
24. Li Z, Guo HJ, Li LZ, et al. Study on surface quality and tool life in ultrasonic vibration countersinking of titanium alloys (Ti6Al4V). *Int J Adv Manuf Technol* 2019;103(1-4):1119-37.
25. Meng D, Liao WH, Dong S. Investigation on fiber fracture mechanisms in rotary ultrasonic milling of carbon fiber reinforced composite. *Int J Adv Manuf Technol* 2023;127(9-10):4877-86.
26. Ji X, Zhang XP, Li BZ, et al. Modeling the Effects of Minimum Quantity Lubrication on Machining Force, Temperature, and Residual Stress. *Int J Precis Eng Man* 2014;18(3-4):547-64.
27. Guo DM, Wen Q, Gao H, et al. Prediction of the cutting forces generated in the drilling of carbon-fibre-reinforced plastic composites using a twist drill. *P I Mech Eng B-J Eng* 2011;226(1):28-42.
28. Machado M, Moreira P, Flores P, et al. Compliant contact force models in multibody dynamics: Evolution of the Hertz contact theory. *Mech Mach Theory* 2012;53(1):99-121.